Dynamics and quantum Zeno effect for a qubit in either a low- or high-frequency bath beyond the rotating-wave approximation

Xiufeng Cao,[1,2,*] J. Q. You,[1,3] H. Zheng,[4] A. G. Kofman,[1,5] and Franco Nori[1,5]

[1]*Advanced Science Institute, RIKEN, Wako-shi 351-0198, Japan*

[2]*Department of Physics and Institute of Theoretical Physics and Astrophysics, Xiamen University, Xiamen, 361005, China*

[3]*Department of Physics and Surface Physics Laboratory (National Key Laboratory), Fudan University, Shanghai 200433, China*

[4]*Department of Physics, Shanghai Jiao Tong University, Shanghai 200240, China*

[5]*Physics Department, The University of Michigan, Ann Arbor, Michigan 48109-1040, USA*

(Received 1 February 2010; published 30 August 2010)

We use a non-Markovian approach to study the decoherence dynamics of a qubit in either a low- or high-frequency bath modeling the qubit environment. This is done for two separate cases: either with measurements or without them. This approach is based on a unitary transformation and does not require the rotating-wave approximation. In the case without measurement, we show that, for low-frequency noise, the bath shifts the qubit energy toward higher energies (blue shift), while the ordinary high-frequency cutoff Ohmic bath shifts the qubit energy toward lower energies (red shift). In order to preserve the coherence of the qubit, we also investigate the dynamics of the qubit subject to measurements (quantum Zeno regime) in two cases: low- and high-frequency baths. For very frequent projective measurements, the low-frequency bath gives rise to the quantum anti-Zeno effect on the qubit. The quantum Zeno effect only occurs in the high-frequency-cutoff Ohmic bath, after counterrotating terms are considered. In the condition that the decay rate due to the two kinds of baths are equal under the Wigner-Weisskopf approximation, we find that without the approximation, for a high-frequency environment, the decay rate should be faster (without measurements) or slower (with frequent measurements, in the Zeno regime), compared to the low-frequency bath case. The experimental implementation of our results here could distinguish the type of bath (either a low- or high-frequency one) and protect the coherence of the qubit by modulating the dominant frequency of its environment.

DOI: 10.1103/PhysRevA.82.022119 PACS number(s): 03.65.Yz, 03.67.−a, 85.25.−j

I. INTRODUCTION

There is considerable interest in low-frequency noise (see, e.g., the review in Ref. [1] and references therein), because this type of noise limits the coherence of qubits based on superconducting devices such as flux or phase qubits [2,3]. Also, the dephasing of flux qubits is due to low-frequency flux noise with intensity comparable to the one measured in dc superconducting quantum interference devives (SQUIDs) (e.g., Refs. [1,4,5]). Under certain conditions, noise can enhance the coherence of superconducting flux qubit (e.g., Ref. [6]. There are also several models (e.g., Refs. [7–9]) for the microscopic origin of low-frequency flux noise in Josephson circuits. Therefore, the study of low-frequency noise has become very important for superconductor qubits [1]. Moreover, the quantum Zeno effect has been proposed as a strategy to protect coherence [10,11] and entanglement [12,13] and to control thermodynamic evolution [14]. The quantum Zeno effect and anti-Zeno effect have been widely discussed [15–17]. So it is an interesting topic to investigate the quantum Zeno effect of a qubit coupled to a low-frequency bath.

The description of low-frequency noise [1] (such as $1/f$ noise) is complicated by the presence of long-time correlations in the fluctuating environment, which prohibit the use of the Markovian approximation. In addition, the rotating-wave approximation (RWA) is also unavailable in an environment with multiple modes [18]. In the case of a time-dependent external field for a qubit coupled to a thermal bath, Kofman and Kurizki developed a theory [19] which considers the counterrotating terms of the fast modulation field through the negative-frequency part $G(\omega)$ ($\omega < 0$) in the bath-correlation function spectrum. The dynamics in two significant models (the spin-boson model with Ohmic bath and a qubit coupled to a bath of two-level fluctuators) have been calculated within a rigorous Born approximation and without the Markovian approximation [20,21]. References [20] and [21] describe the structure of the solutions in the complex plane with branch cuts and poles.

Here we present an analytical approach, based on a unitary transformation. We use neither the Markovian approximation nor the RWA in order to discuss the transient dynamics of a qubit coupled to its environment. This method has already been used [22] to study the decoherence of the Ohmic bath, sub-Ohmic bath, and structured bath. In this paper, we calculate the coherence dynamics of the qubit respectively in two kinds of baths. This is done for two separate cases: either with measurements or without them. Besides producing an energy shift, the environment can change the decay rate of the qubit. To preserve the coherence, we also investigate the decay rate of the qubit subject to the quantum Zeno effect. The low-frequency noise uses a Lorentzian-type spectrum, with the peak of the spectrum in the low-energy region, and for the high-frequency noise we choose an ordinary Ohmic bath with Drude cutoff.

Our results show that for *low*-frequency noise, the qubit energy increases (blue shift) and an anti-Zeno effect takes place. For a *high*-frequency cutoff Ohmic bath, the qubit

*xfcao@xmu.edu.cn

energy decreases (red shift) and the Zeno effect dominates. In the condition that the decay rate owing to the two kinds of baths are equal under the Wigner-Weisskopf (WW) approximation, we find that without the approximation, for a high-frequency environment, the decay rate should be faster (without measurements) or slower (with frequent measurements, in the Zeno regime), compared to the low-frequency bath case. This means that without measurement, the coherence time of the low-frequency noise is longer than the high-frequency noise, $\tau_{\text{coherence}}^{(\text{low freq})} > \tau_{\text{coherence}}^{(\text{high freq})}$. This demonstrates the powerful temporal memory of the low-frequency bath and stems from non-Markovian processes of qubit-bath interaction within the bath memory time [23]. The experimental implementation of our results here could distinguish the type of bath (either a low- or high-frequency one) and protect the coherence of the qubit by modulating the dominant frequency of its environment.

II. METHOD BEYOND THE RWA BASED ON A UNITARY TRANSFORMATION

We describe a qubit coupled to a boson bath, modeling the environment, by the Hamiltonian

$$H = -\frac{1}{2}\Delta\sigma_z + \frac{1}{2}\sum_k g_k(a_k^\dagger + a_k)\sigma_x + \sum_k \omega_k a_k^\dagger a_k. \quad (1)$$

The boson bath and the spin-$\frac{1}{2}$ (fluctuators) bath will have the same dissipative effect on the qubit at zero temperature, $T = 0$, if both baths have the same correlation function [24]. However, for finite temperatures, the spin bath has a smaller effect on the qubit because of the likely saturation of the populations in the spin bath. Here, for simplicity, we only consider the case of zero temperature. That is, our results are also applicable to a fluctuator-bath at zero temperature. Our approach is based on a unitary transformation and can be used for different types of environmental baths. In the following we give detailed derivations for the low-frequency noise case.

The spectral density $J(\omega)$ of the environment considered here is given by

$$J(\omega) = \sum_k g_k^2\delta(\omega - \omega_k) = \frac{2\alpha\omega}{\omega^2 + \lambda^2}, \quad (2)$$

where λ is an energy lower than the qubit two-energy spacing Δ and α describes the coupling strength between the qubit and the environment. By choosing Δ as the energy unit, α/Δ^2 is a dimensionless coupling strength. When $\omega \geqslant \lambda$, $J(\omega) \sim 1/\omega$, corresponding to a $1/f$ noise.

To take account of the counterrotating terms in $\sum_k g_k(a_k^\dagger + a_k)\sigma_x$, we apply a canonical transformation to the Hamiltonian H:

$$H' = \exp(S)H\exp(-S), \quad (3)$$

with $S = \sum_k \frac{g_k}{2\omega_k}\xi_k(a_k^\dagger - a_k)\sigma_x$, $\xi_k = \omega_k/(\omega_k + \eta\,\Delta)$, and

$$\eta = \exp\left(-\sum_k \frac{g_k^2}{2\omega_k^2}{\xi_k}^2\right). \quad (4)$$

Further explanations on the validity of the transformation can be found in the Appendix. Thus, the effective transformed Hamiltonian can be derived as (see the Appendix)

$$H' \approx -\frac{1}{2}\eta\,\Delta\sigma_z + \sum_k \omega_k a_k^\dagger a_k + \sum_k V_k(a_k^\dagger\sigma_- + a_k\sigma_+), \quad (5)$$

with

$$V_k = \eta\,\Delta\frac{g_k\xi_k}{\omega_k}. \quad (6)$$

Comparing H' in Eq. (5) with the ordinary Hamiltonian in the RWA,

$$H_{\text{RWA}} = -\frac{1}{2}\Delta\sigma_z + \sum_k \omega_k a_k^\dagger a_k + \sum_k \frac{g_k}{2}(a_k^\dagger\sigma_- + a_k\sigma_+), \quad (7)$$

one can see that the unitary transformation plays the role of renormalizing two parameters in the Hamiltonian; that is, the energy spacing Δ is renormalized,

$$\Delta \longrightarrow \eta\,\Delta, \quad (8)$$

and the coupling strength $g_k/2$ between the qubit and the bath is renormalized,

$$\frac{g_k}{2} \longrightarrow \left(\frac{2\eta\,\Delta}{\omega_k + \eta\,\Delta}\right)\frac{g_k}{2}. \quad (9)$$

In the following we will study the decoherence dynamics of the qubit and the quantum Zeno effect using the transformed Hamiltonian H'.

Note that the term $\sum_k g_k^2{\xi_k}^2/(2\omega_k^2)$ in Eq. (4) is larger than 0, so $0 < \exp[-\sum_k g_k^2{\xi_k}^2/(2\omega_k^2)] < 1$. Then the solution of η will be in the region from 0 to 1. Actually, the existence and uniqueness of the solution of η in Eq. (4) can be used as a criterion for the validity of our method. The parameter η can be regarded as a renormalization factor of the energy spacing Δ and is calculated as

$$\eta = \exp\left\{\frac{\alpha\left[\pi\lambda\eta\,\Delta - \lambda^2 - \eta^2\Delta^2 + (\lambda^2 - \eta^2\Delta^2)\log\left|\frac{\lambda}{\eta\,\Delta}\right|\right]}{(\lambda^2 + \eta^2)^2}\right\}. \quad (10)$$

Obviously, η is determined self-consistently by this equation.

A. Nonmeasurement decoherence dynamics

Let us first consider the dynamics without measurement. We diagonalize the transformed Hamiltonian H' in the ground state $|g\rangle = |\uparrow\rangle|\{0_k\}\rangle$ and lowest excited states, $|\downarrow\rangle|\{0_k\}\rangle$ and $|\uparrow\rangle|1_k\rangle$, as

$$H' = -\frac{1}{2}\eta\,\Delta|g\rangle\langle g| + \sum_E E|E\rangle\langle E|, \quad (11)$$

where $|\uparrow\rangle$ and $|\downarrow\rangle$ are the eigenstates of σ_z, that is, $\sigma_z|\uparrow\rangle = |\uparrow\rangle$, $\sigma_z|\downarrow\rangle = -|\downarrow\rangle$, and $|n_k\rangle$ denotes the state with n bath excitations for mode k. The state $|E\rangle$ is

$$|E\rangle = x(E)\,|\downarrow\rangle\,|\{0_k\}\rangle + \sum_k y_k(E)|\uparrow\rangle|1_k\rangle, \quad (12)$$

with $x(E)=[1+\sum_k \frac{V_k^2}{(E+\eta\Delta/2-\omega_k)^2}]^{-1/2}$ and $y_k(E)=\frac{V_k}{E+\eta\Delta/2-\omega_k}x(E)$.

Here we calculate the dynamical quantity $\langle\sigma_x(t)\rangle$, which is the analog of the population inversion $\langle\sigma_z(t)\rangle$ in the spin-boson model [25]. Since the coupling to the environment will be "always present" in essentially all physically relevant situations, a natural ground state is given by the dressed state of the two-level qubit and bath. Therefore, by considering the counterrotating terms, the ground state of H is a dressed state $\exp[-S]|\uparrow\rangle|\{0_k\}\rangle$ [26], and the corresponding ground-state energy is $-\eta\,\Delta/2$, so the ground state of H' becomes $|\uparrow\rangle|\{0_k\}\rangle$ with the identical ground-state energy, $-\eta\,\Delta/2$. We now prepare the initial state, which is also a dressed state of the qubit and bath, from the ground state as

$$|\psi(0)\rangle=\frac{(1+\sigma_x)}{\sqrt{2}}\exp[-S]|\uparrow\rangle|\{0_k\}\rangle. \tag{13}$$

Then the initial state in the *transformed Hamiltonian* becomes $|\psi'(0)\rangle=(|\uparrow\rangle+|\downarrow\rangle)|\{0_k\}\rangle/\sqrt{2}$, which is the eigenstate of σ_x. Starting from this initial state, we obtain [27]

$$\begin{aligned}\langle\sigma_x(t)\rangle &= \mathrm{Tr}_B\,\langle\psi(t)\,|\sigma_x|\,\psi(t)\rangle\\ &= \mathrm{Tr}_B\langle\psi(0)|\exp(iHt)\sigma_x\exp(-iHt)|\psi(0)\rangle\\ &= \frac{1}{2}\sum_E x(E)^2\exp\left[-i\left(E+\frac{\eta\,\Delta}{2}\right)t\right]\\ &\quad+\frac{1}{2}\sum_E x(E)^2\exp\left[i\left(E+\frac{\eta\,\Delta}{2}\right)t\right]\\ &= \int_\infty^{-\infty}\frac{dE'}{4\pi i}\exp(-iE't)\\ &\quad\times\left(E'-\eta\,\Delta-\sum_k\frac{V_k^2}{E'+i0^+-\omega_k}\right)^{-1}\\ &\quad+\int_{-\infty}^{\infty}\frac{dE'}{4\pi i}\exp(iE't)\\ &\quad\times\left(E'-\eta\,\Delta-\sum_k\frac{V_k^2}{E'-i0^+-\omega_k}\right)^{-1}\\ &= \mathrm{Re}\left[\frac{1}{2\pi i}\int_\infty^{-\infty}\frac{\exp(-iE't)}{E'-\eta\,\Delta-\sum_k\frac{V_k^2}{E'+i0^+-\omega_k}}dE'\right].\end{aligned} \tag{14}$$

Here we denote the real and imaginary parts of $\sum_k V_k^2/(\omega-\omega_k\pm i0^+)$ as $R(\omega)$ and $\mp\Gamma(\omega)$, respectively. It follows that

$$\begin{aligned}R(\omega)&=\wp\sum_k\frac{V_k^2}{\omega-\omega_k}=(\eta\,\Delta)^2\wp\int_0^\infty d\omega'\frac{J(\omega')}{(\omega-\omega')(\omega'+\eta\,\Delta)^2}=2\alpha\Delta^2\eta^2\frac{\omega\log|\omega|}{(\eta\,\Delta+\omega)^2(\lambda^2+\omega^2)}\\&+2\alpha\Delta^2\eta^2\frac{\pi\lambda[\lambda^2+\eta\,\Delta\,(-\eta\,\Delta+2\omega)]-2[\lambda^2(2\eta\,\Delta-\omega)+\eta^2\,\Delta^2\,\omega]\log|\lambda|}{2(\lambda^2+\eta^2\Delta^2)^2(\lambda^2+\,\omega^2)}\\&+2\alpha\Delta^2\eta^2\frac{-(\eta\,\Delta+\omega)(\lambda^2+\Delta^2\eta^2)+[2\eta^3\Delta^3+(-\lambda^2+\eta^2\Delta^2)\,\omega]\log|\eta\,\Delta|}{(\lambda^2+\eta^2\Delta^2)^2(\eta\,\Delta+\omega)^2}\end{aligned} \tag{15}$$

and

$$\Gamma(\omega)=\pi\sum_k V_k^2\delta(\omega-\omega_k)=\pi(\eta\,\Delta)^2\frac{J(\omega)}{(\omega+\eta\,\Delta)^2}, \tag{16}$$

where $\wp$ stands for the Cauchy principal value and $J(\omega)$ is the spectral density. Then, we have

$$\langle\sigma_x(t)\rangle=\frac{1}{\pi}\int_0^\infty\frac{\Gamma(\omega)\cos\omega t}{[\omega-\eta\,\Delta-R(\omega)]^2+\Gamma(\omega)^2}d\omega. \tag{17}$$

The integration in Eq. (17) can be calculated numerically or approximately using residual theory.

B. Measurement dynamics: quantum Zeno effect

It is known that the quantum Zeno effect can effectively slow down the quantum decay rate of a quantum system. We study this effect using an approach that goes beyond the RWA. Here we consider the low-frequency bath as in Sec. II A and derive the effective decay rate. The Hamiltonian H' is given in Eq. (5).

Let us write the wave function in the transformed Hamiltonian as

$$|\Phi'(t)\rangle=\chi(t)\,|\downarrow\rangle\,|\{0_k\}\rangle+\sum_k\beta_k(t)\,|\uparrow\rangle\,|1_k\rangle\,, \tag{18}$$

with probability in the excited state at the initial time $|\chi(0)|^2$. We have demonstrated that the ground state of Hamiltonian (1) is a dressed state $\exp(-S)|\uparrow\rangle|\{0_k\}\rangle$ in the previous section. Now we prepare the qubit to the dressed excited state $\exp(-S)|\downarrow\rangle|\{0_k\}\rangle$ ($\sigma_z|\downarrow\rangle=-|\downarrow\rangle$) at the initial time $t=0$, which can be achieved by acting the operator σ_x on the ground state,

$$|\Phi(0)\rangle=\sigma_x\exp(-S)|\uparrow\rangle|\{0_k\}\rangle=\exp(-S)|\downarrow\rangle|\{0_k\}\rangle. \tag{19}$$

In this case, the initial state in the transformed Hamiltonian is $|\downarrow\rangle|\{0_k\}\rangle$ and $\chi(0)=1$. Substituting $|\Phi'(t)\rangle$ into the

Schrödinger equation with H', we have

$$i\frac{d\chi(t)}{dt} = \frac{\eta\,\Delta}{2}\chi(t) + \sum_k V_k\,\beta_k(t), \tag{20}$$

$$i\frac{d\beta_k(t)}{dt} = \left(\omega_k - \frac{\eta\,\Delta}{2}\right)\beta_k(t) + \sum_k V_k\,\chi(t). \tag{21}$$

When the transformations

$$\chi(t) = \widetilde{\chi}(t)\exp\left(-i\frac{\eta\,\Delta}{2}t\right), \tag{22}$$

$$\beta_k(t) = \widetilde{\beta}_k(t)\exp\left[-i\left(\omega_k - \frac{\eta\,\Delta}{2}\right)t\right] \tag{23}$$

are applied, Eqs. (20) and (21) can be written as

$$\frac{d\widetilde{\chi}(t)}{dt} = -i\sum_k V_k\widetilde{\beta}_k(t)\exp[-i(\omega_k - \eta\,\Delta)t], \tag{24}$$

$$\frac{d\widetilde{\beta}_k(t)}{dt} = -i\,V_k\widetilde{\chi}(t)\exp[i(\omega_k - \eta\,\Delta)t]. \tag{25}$$

Integrating Eq. (25) and then substituting it into Eq. (24), we obtain

$$\frac{d\widetilde{\chi}(t)}{dt} = -\sum_k V_k^2\int_0^t \widetilde{\chi}(t')\exp[-i(\omega_k - \eta\,\Delta)(t-t')]\,dt'. \tag{26}$$

This integro-differential equation (26) is exactly soluble by a Laplace transformation.

As for the present study of the quantum Zeno effect (i.e., using frequent measurements [28,29]), it suffices to obtain the short-time behavior and the equation can be solved iteratively. With the initial excited-state probability amplitude $\chi(0)$, in the first iteration, Eq. (26) is solved as

$$\widetilde{\chi}(t) \simeq 1 - \int_0^t (t-t')\sum_k V_k^2\exp[-i(\omega_k - \eta\,\Delta)t']\,dt'. \tag{27}$$

We can approximately write $\widetilde{\chi}(t)$ using an exponential form:

$$\widetilde{\chi}(t) = \exp\left[-\int_0^t (t-t')\sum_k V_k^2\exp[-i(\omega_k - \eta\,\Delta)t']\,dt'\right] \tag{28}$$

$$= \exp\left\{-t\left[-\frac{1}{t}\sum_k V_k^2\frac{\exp[-i\,(\omega_k - \eta\,\Delta)\,t] - 1 + i\,(\omega_k - \eta\,\Delta)\,t}{(\omega_k - \eta\,\Delta)^2}\right]\right\} \tag{29}$$

$$= \exp\left\{-t\left[\sum_k V_k^2\left(\frac{2\sin\left(\frac{\omega_k - \eta\,\Delta}{2}t\right)^2}{t\,(\omega_k - \eta\,\Delta)^2} - i\frac{(\omega_k - \eta\,\Delta)\,t - \sin[(\omega_k - \eta\,\Delta)\,t]}{t\,(\omega_k - \eta\,\Delta)^2}\right)\right]\right\}. \tag{30}$$

Assuming we perform the instantaneous ideal projections to the initial state at intervals τ, for a single measurement, the probability amplitude is $\widetilde{\chi}(t=\tau)$. For a sufficiently large frequency of measurements, the survival population in the excited state [30] is

$$\rho_{\rm ee}(t = n\tau) = |\widetilde{\chi}(t = n\tau)|^2 = \exp[-\gamma(\tau)t], \tag{31}$$

where the subscript "ee" refers to the initial and final excited state. The decay rate $\gamma(\tau)$, with projection intervals τ, is obtained as

$$\gamma(\tau) = 2\pi\int_0^\infty d\omega\sum_k\left(\frac{g_k}{2}\right)^2\left(\frac{2\eta\,\Delta\xi_k}{\omega_k}\right)^2\frac{2\sin^2\left(\frac{\eta\,\Delta-\omega}{2}\tau\right)}{\pi(\eta\Delta-\omega)^2\tau}$$

$$= 2\pi\int_0^\infty d\omega\frac{J(\omega)}{4}\left[1 - \frac{\omega - \eta\,\Delta}{\omega + \eta\,\Delta}\right]^2\frac{2\sin^2\left(\frac{\eta\,\Delta-\omega}{2}\tau\right)}{\pi(\eta\Delta-\omega)^2\tau}. \tag{32}$$

Note that, in Eq. (32), the renormalization factor η of the characteristic energy Δ appears in the decay rate $\gamma(\tau)$. This is different from the formulas for $\gamma(\tau)$ in Refs. [30,31]. In the case of spontaneous emission, the coupling strength between the electromagnetic field and atom is the fine-structure constant $1/137$, so it belongs to the weak-coupling case and η then becomes extremely close to 1. Therefore, besides spontaneous emission, this result for the quantum Zeno effect can apply to other cases of strong coupling between the qubit and the bath.

Under the RWA, the Hamiltonian becomes $H_{\rm RWA}$ as in Eq. (7). We prepare the initial excited state of H through the operator σ_x acting on the ground state under RWA $|\uparrow\rangle|\{0_k\}\rangle$, $\sigma_x|\uparrow\rangle|\{0_k\}\rangle = |\downarrow\rangle|\{0_k\}\rangle$. Then, following the derivation in Refs. [15], the decay rate is reduced to

$$\gamma_{\rm RWA}(\tau) = 2\pi\int_0^\infty d\omega\sum_k\left(\frac{g_k}{2}\right)^2\frac{2\sin^2\left(\frac{\Delta-\omega}{2}\tau\right)}{\pi(\Delta-\omega)^2\tau}$$

$$= 2\pi\int_0^\infty d\omega\frac{J(\omega)}{4}\frac{2\sin^2\left(\frac{\Delta-\omega}{2}\tau\right)}{\pi(\Delta-\omega)^2\tau}. \tag{33}$$

To compare with the high-frequency bath, we choose the ordinary Ohmic bath with Drude cutoff:

$$J^{\rm Ohm}(\omega) = \sum_k g_k^2\delta(\omega - \omega_k) = \frac{2\alpha^{\rm Ohm}\omega}{(\omega/\omega_c)^2 + 1}. \tag{34}$$

This is a realistic assumption for, for example, electromagnetic noise. In Eq. (34), $\alpha^{\rm Ohm}$ is the coupling strength between the qubit and the Ohmic bath. The cutoff frequency ω_c in the spectral density $J^{\rm Ohm}(\omega)$ is typically assumed to be the largest frequency in the problem. As for the low-frequency noise, we

use $J(\omega) = 2\alpha\omega/(\omega^2 + \lambda^2)$, which is the same as in Eq. (2). The difference between these two baths is that λ corresponds to an energy lower than the qubit energy. In the next section, we will show our numerical results for these two baths.

III. RESULTS AND DISCUSSION

To show the effects of either a low- or a high-frequency noise on the qubit states respectively, we study the dynamical quantities $\langle\sigma_x(t)\rangle$ and the quantum Zeno decay rate $\gamma(\tau)$. The energy shift and the quantum Zeno decay rate exhibit evidently different features for the low- and high-frequency noises. Thus, these two quantities (energy shift and decay rate) can be used as criteria to distinguish the type of noise. In Fig. 1, we show the spectral densities $J(\omega)$ and $J^{\rm Ohm}(\omega)$ of the two baths in the cases of both weak dissipation, $\alpha/\Delta^2 = 0.01$ ($\alpha^{\rm Ohm} = 0.01$), and strong dissipation, $\alpha/\Delta^2 = 0.1$ ($\alpha^{\rm Ohm} = 0.1$). As examples, we choose $\lambda = 0.09\Delta$ and $\lambda = 0.3\Delta$ in Figs. 1(a) and 1(b), respectively. Here, each value of λ corresponds to the position of the peak in the low-frequency spectral density. In superconducting qubits, the low-frequency cutoff for $1/f$ noise is bounded from the repetition rate of the experiments and this can be as low as 1 Hz [32]. For example, we calculated the case when $\lambda = 10^{-10}\Delta$ (which corresponds to $\lambda = 1$ Hz and $\Delta = 10$ GHz) and found that there is no substantial difference with the following results. Thus, our results are relevant for superconducting qubits. For an Ohmic bath, the cutoff frequency is fixed at $\omega_c = 10\Delta$. As expected, these very different low- and high-frequency spectral densities should give rise to different decoherence behaviors of the qubit. In Fig. 1, we also show the characteristic energy of the isolated qubit Δ (see the vertical dotted line in Fig. 1).

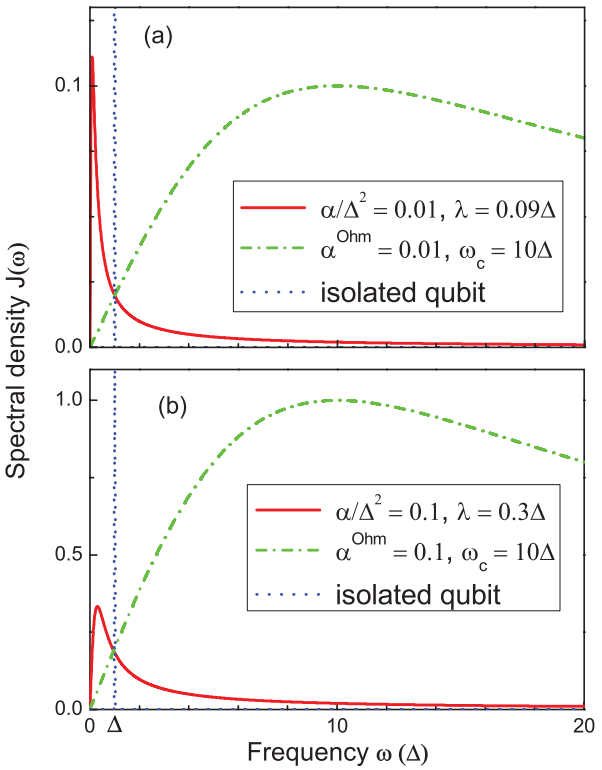

FIG. 1. (Color online) The spectral density $J(\omega)$ of the low- and high-frequency baths. (a) The case of *weak* interaction between the bath and the qubit, where the parameters of the low-frequency Lorentzian-like spectrum are $\alpha/\Delta^2 = 0.01$ and $\lambda = 0.09\Delta$ (red solid curve), while for the high-frequency Ohmic bath with Drude cutoff the parameters are $\alpha^{\rm Ohm} = 0.01$ and $\omega_c = 10\Delta$ (green dashed-dotted curve). (b) The case of *strong* interaction between the bath and the qubit, where the parameters of the low-frequency bath are $\alpha/\Delta^2 = 0.1$ and $\lambda = 0.3\Delta$ (red solid curve) and the parameters of the high-frequency Ohmic bath are $\alpha^{\rm Ohm} = 0.1$ and $\omega_c = 10\Delta$ (green dashed-dotted curve). The characteristic energy of the isolated qubit is indicated by a vertical blue dotted line. Here, and in the following figures, the energies are shown in units of Δ.

A. Nonmeasurement decoherence dynamics

Now let us consider the dynamics without measurements. Results from the numerical integration of Eq. (17) are shown in Fig. 2. They are qualitatively consistent with the results obtained using residual theory. This indicates that the branch cuts considered in Refs. [20] and [21] do not affect the oscillation frequency. The time evolution of $\langle\sigma_x(t)\rangle$ is given in Fig. 2(a) for the case of weak coupling between the qubit and the bath, where $\alpha/\Delta^2 = 0.01$ and $\lambda = 0.09\Delta$ for the low-frequency noise and $\alpha^{\rm Ohm} = 0.01$ and $\omega_c = 10\Delta$ for the Ohmic bath. Figure 2(b) presents the time evolution of $\langle\sigma_x(t)\rangle$ in the strong-coupling case with the parameters $\alpha/\Delta^2 = 0.1$ and $\lambda = 0.3\Delta$ for the low-frequency noise, as well as $\alpha^{\rm Ohm} = 0.1$ and $\omega_c = 10\Delta$ for the Ohmic bath. As expected, the quantum oscillations of $\langle\sigma_x(t)\rangle$ dampen faster in the strong-coupling case. We approximately evaluate the oscillation frequency or the effective energy of the qubit, $\omega_0 - \eta\Delta - R(\omega_0) = 0$, using the residue theorem. The decay rate can be obtained from $\Gamma(\omega)$. We will now show the numerical values of η in the corresponding cases. In Fig. 2(a), the renormalized factor $\eta = 0.98336$, the oscillation frequency is $\omega_0 = 1.0225\Delta$, and the decay rate is $\Gamma(\omega_0) = 0.014654\Delta$ for the low-frequency noise; $\eta = 0.98447$, $\omega_0 = 0.97720\Delta$, and $\Gamma(\omega_0) = 0.015318\Delta$ for the Ohmic bath. In Fig. 2(b), the renormalized factor $\eta = 0.91444$, the oscillation frequency is $\omega_0 = 1.0868\Delta$, and the decay rate is $\Gamma(\omega_0) = 0.11215\Delta$ for the low-frequency noise, while $\eta = 0.84469$, $\omega_0 = 0.77221\Delta$, and $\Gamma(\omega_0) = 0.13163\Delta$ for the Ohmic bath.

The energy spectral densities in Fig. 1 and the results in Fig. 2 indicate two opposite shifts of the characteristic energy Δ for the two kinds of baths considered here. These opposite energy shifts are equivalent to energy repulsion. The energy shift is determined by the interaction term. In the transformed Hamiltonian, the interaction term is H_1' in Eq. (A5). Also, dipolar interactions, such as $H_I^{\rm JC} = g(a^\dagger\sigma_- + a\sigma_+)$ in the Jaynes-Cummings model, decrease the qubit's ground-state energy and increase its excited-state energy. Thus, now we ask the following questions: What is the difference of a qubit affected by either a multimode bath or a single-mode cavity? How is a qubit influenced by these two kinds of multimode baths (low-frequency and high-frequency ones)?

For a low-frequency bath, the energy peak of the bath is located between the ground-state energy ($\omega = 0$) and the excited-state energy ($\omega = \Delta$); that is, the main part of the spectrum is in the region $\omega_k < \Delta$. Then (as seen in Fig. 1) the interaction of the bath with the two qubit states is "opposite" (i.e., the ground-state energy becomes lower and the

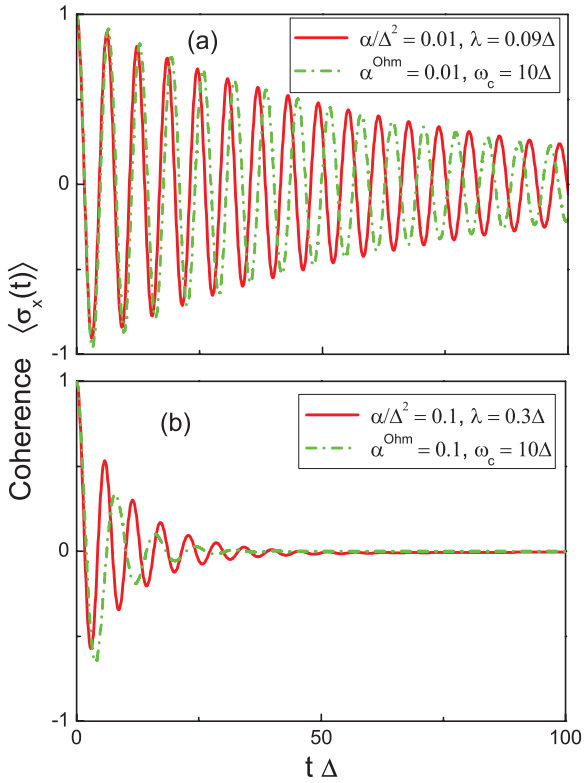

FIG. 2. (Color online) Time evolution of the coherence $\langle\sigma_x(t)\rangle$ versus the time t multiplied by the qubit energy spacing Δ. (a) The case of *weak* interaction between the bath and the qubit, where the parameters of the low-frequency Lorentzian-type spectrum are $\alpha/\Delta^2 = 0.01$ and $\lambda = 0.09\Delta$ (red solid curve), while for the high-frequency Ohmic bath with Drude cutoff the parameters are $\alpha^{\rm Ohm} = 0.01$ and $\omega_c = 10\Delta$ (green dashed-dotted curve). (b) The case of *strong* interaction between the bath and the qubit, where the parameters of the low-frequency bath are $\alpha/\Delta^2 = 0.1$ and $\lambda = 0.3$ (red solid line), and for the high-frequency Ohmic bath the parameters are $\alpha^{\rm Ohm} = 0.1$ and $\omega_c = 10\Delta$ (green dashed-dotted line). These results show that under the condition that the decay rates of two kinds of baths are equal in the WW approximation, by considering the counterrotating terms, the decay rate for the low-frequency bath is *smaller* than that for the high-frequency Ohmic bath. This means that the coherence time of the qubit in the low-frequency bath is *longer* than in the high-frequency-noise case, demonstrating the powerful temporal memory of the low-frequency bath. Also, our results reflect the structure of the solution with branch cuts [20]. The oscillation frequency for the low-frequency noise is $\omega_0 > \Delta$, in spite of the strength of the interaction. This can be referred to as a blue shift. However, in an Ohmic bath, the oscillation frequency is $\omega_0 < \Delta$, corresponding to a red shift. The shifting direction of the energy is independent of the interaction strength and only determined by the spectral properties. Thus, it can be used as a criterion for distinguishing the low- and high-frequency noises.

excited-state energy becomes higher). So the energy spacing for the case of a low-frequency bath exhibits a *blue shift*. This result is similar to the single-mode Jaynes-Cummings model. The energy difference of the two-state qubit is increased by the low-frequency bath.

For a high-frequency cutoff Ohmic bath, the energy peak of the bath is located above the excited-state energy. So the main part of the spectrum is in the region $\omega_k > \Delta$. The effect of the bath on the qubit mainly comes from the frequencies higher than the excited-state energy of the qubit. Then (as seen in Fig. 1) the bath repels both the excited-state and the ground-state energies to lower energies. But the effect of the high-frequency bath on the excited state is much larger than on the ground state. As a result, on the whole, the qubit energy difference in a high-frequency bath is *red shifted*. Thus, the effective energy difference of the qubit is reduced by the high-frequency bath.

For example, if the initial state of the qubit is an excited state, in the interaction picture, the main part of the coupling is

$$\sum_k g_k a_k^\dagger \exp(i\omega_k t)\sigma_- \exp(-i\Delta t) = \sum_k g_k a_k^\dagger \sigma_- \{\cos[(\omega_k - \Delta)t] + i\sin[(\omega_k - \Delta)t]\}, \quad (35)$$

where the real part contributes to the decay rate and the imaginary part results in the energy shift. For the low-frequency bath, the main part of the spectrum is in the region $\omega_k < \Delta$. Thus, the term for the energy shift is

$$\sin[(\omega_k - \Delta)t] < 0. \quad (36)$$

However, for a high-frequency-cutoff Ohmic bath, the main part of the spectrum is in the region $\omega_k > \Delta$, where the term for energy shift becomes

$$\sin[(\omega_k - \Delta)t] > 0. \quad (37)$$

These results show that the energy shift for the two kinds of baths moves in opposite directions. Note that there is a minus sign in the interaction term in the expressions for the dynamical quantities such as Eq. (14) and Eq. (26). These observations help us understand why the energy levels repel. The contribution by the real part of the interaction on the decay rate will be discussed next, when studying the quantum Zeno effect.

B. Measurement dynamics: quantum Zeno effect

Now let us consider the case with measurements [28]. The quantum Zeno effect can be a useful tool to preserve the state coherence of a quantum system, with the help of repeated projective measurements. In the following we investigate the quantum Zeno effect in the qubit system and propose another criterion for distinguishing low- and high-frequency noises. In general, without using the RWA, the decay rate under measurement can be obtained as

$$\gamma(\tau) = 2\pi \int_0^\infty d\omega J(\omega) \left(1 - \frac{\omega - \eta\ \Delta}{\omega + \eta\ \Delta}\right)^2 \frac{2\sin^2\left(\frac{\eta\ \Delta - \omega}{2}\tau\right)}{\pi(\eta\ \Delta - \omega)^2\tau}. \quad (38)$$

This expression includes three terms, that is, the spectral density $J(\omega)$ of the bath, the projection time modulating function

$$F(\omega,\tau) = \frac{2\sin^2\left(\frac{\eta\ \Delta - \omega}{2}\tau\right)}{\pi(\eta\ \Delta - \omega)^2\tau}, \quad (39)$$

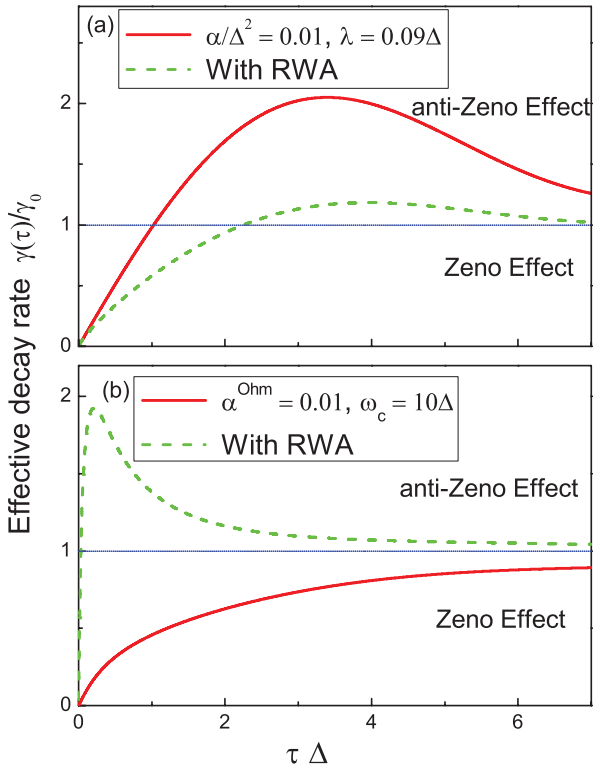

FIG. 3. (Color online) The effective decay $\gamma(\tau)/\gamma_0$, versus the time interval τ between consecutive measurements for a *weak* coupling between the qubit and the bath. On the horizontal axis, the time interval τ is multiplied by the qubit energy difference Δ. The curves in (a) correspond to the case of a low-frequency bath with parameters $\alpha/\Delta^2 = 0.01$ and $\lambda = 0.09\Delta$ (red solid curve); the curves in (b) correspond to the case of an Ohmic bath with parameters $\alpha^{\rm Ohm} = 0.01$ and $\omega_c = 10\Delta$ (red solid curve). The green dashed-dotted curves are the results under the RWA when the same parameters are used. Note how different the RWA result is in (b), especially for any short measurement interval τ.

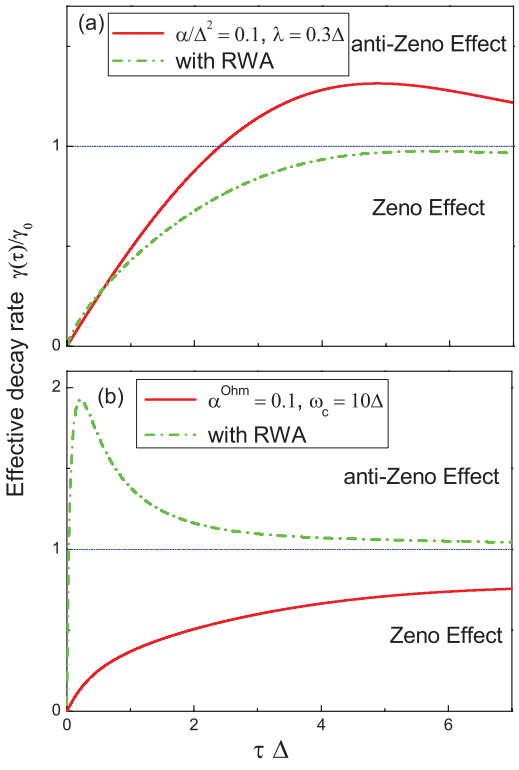

FIG. 4. (Color online) The effective decay $\gamma(\tau)/\gamma_0$, versus the time interval τ between successive measurements for a *strong* coupling between the qubit and the bath. The time interval τ is multiplied by the qubit energy difference Δ. The curves in (a) correspond to the case of a low-frequency bath with parameters $\alpha/\Delta^2 = 0.1$ and $\lambda = 0.3\Delta$ (red solid curve); the curves in (b) correspond to the case of an Ohmic bath with parameters $\alpha^{\rm Ohm} = 0.1$ and $\omega_c = 10\Delta$ (red solid curve). The green dashed-dotted curves are the results under RWA when the same parameters are used. Note how different the RWA result is in (b), especially for any short measurement interval τ.

and the interaction contribution function of both the rotating and counterrotating terms,

$$f(\omega) = \left(1 - \frac{\omega - \eta\ \Delta}{\omega + \eta\ \Delta}\right)^2. \tag{40}$$

The counterrotating term contributing to $f(\omega)$ is $(\omega - \eta\ \Delta)/(\omega + \eta\ \Delta)$. If the RWA is applied, $f(\omega) = 1$. The decay rate for $|e\rangle \to |g\rangle$ in the long-time limit, corresponding to the decay rate under the WW approximation, is written as γ_0:

$$\gamma_0 = \gamma(\tau \to \infty) = 2\pi J(\Delta)/4. \tag{41}$$

The effective decay rate is the ratio of $\gamma(\tau)$ to γ_0, which is in the same form as in Ref. [15]. In Fig. 3(a), the effective decay rate $\gamma(\tau)/\gamma_0$ for the low-frequency bath is plotted in the weak-coupling case with $\alpha/\Delta^2 = 0.01$. From the energy spectrum in Fig. 1(a), we can see that γ_0 is proportional to the spectrum density of the bath, with the magnitude corresponding to the crossing of the energy Δ of the isolated qubit and the bath spectrum. For comparison, we also plot $\gamma_{\rm RWA}(\tau)/\gamma_0$ as a dashed-dotted curve, with

$$\gamma_{\rm RWA}(\tau) = 2\pi \int_0^\infty d\omega \frac{J(\omega)}{4} \frac{2\sin^2\left(\frac{\Delta-\omega}{2}\tau\right)}{\pi(\Delta-\omega)^2\tau}. \tag{42}$$

As we know, $\gamma(\tau)/\gamma_0 < 1$ means that repeated measurements slow down the decay rate $\gamma(\tau) < \gamma_0$, which is the quantum Zeno effect. In contrast, $\gamma(\tau)/\gamma_0 > 1$ means an anti-Zeno effect. The curves in Fig. 3(b) show results for the Ohmic bath with $\alpha^{\rm Ohm} = 0.01$. In Fig. 4, we show the decay rate in the strong-coupling case for the low-frequency bath with $\alpha/\Delta^2 = 0.1$ and for the Ohmic bath with $\alpha^{\rm Ohm} = 0.1$. It can be seen that, for the low-frequency bath, the anti-Zeno effect appears as shown in Figs. 3 and 4. For the high-frequency-cutoff Ohmic bath, the Zeno effect always dominates and no anti-Zeno effect occurs. Also we can see, from Figs. 3 and 4, that $\gamma(\tau)$ and $\gamma_{\rm RWA}(\tau)$ approach γ_0 when the measurement interval $\tau \to \infty$. In particular, if $\tau \to 0$, $F(\omega,\tau) \to 0$. Thus, $\gamma(\tau) \to 0$. This implies that, in a sufficiently short time interval of a projective measurement, the quantum Zeno effect occurs, regardless of the bath spectrum. When the interval τ increases, the projection interval modulation function $F(\omega,\tau)$ displays a number of oscillations. Then, the energy peak of the bath spectrum will act on the decay rate and it is

TABLE I. Summary of our main results for the quantum Zeno effect (QZE) and anti-Zeno effect (AZE), with and without RWA. The entries in the last column marked by an asterisk indicate which changes in the dynamics (Zeno versus anti-Zeno) are related to using the RWA. Here, α describes the coupling strength between the qubit and the environment. The system dynamics can be either quantum Zeno or anti-Zeno depending on several factors, including the type of bath, the strength of the qubit-bath coupling, the frequency of the measurements, etc. These results are described in detail in the main text.

Bath	Coupling α	Measurement frequency $\sim \tau^{-1}$	Without RWA $t = 0$ dressed state	RWA $t = 0$ product state
Low-frequency	0.1	high	QZE	QZE
		low	AZE	*QZE
	0.01	high	QZE	QZE
		low	AZE	AZE
Ohmic	0.1	high	QZE	QZE
		low	QZE	*AZE
	0.01	high	QZE	QZE
		low	QZE	*AZE

possible to implement the anti-Zeno effect. However, this result still depends on the function $f(\omega)$ and the given spectral density $J(\omega)$ of the bath. Now, we emphasize again that the second term in the brackets of the function $f(\omega) = [1 - (\omega - \eta\ \Delta)/(\omega + \eta\ \Delta)]^2$ is due to the counterrotating terms; when neglecting the counterrotating terms, $f(\omega) = 1$.

For low-frequency noise, the noise mainly comes from the region $\omega < \Delta$, so $f(\omega) > 1$. Here, $f(\omega)$ as well as $F(\omega,\tau)$ magnify the effect of the energy peak of the bath spectrum. Thus, the counterrotating terms accelerate the decay and the anti-Zeno effect occurs.

In the high-frequency-cutoff Ohmic bath, the noise mainly comes from the region $\omega > \Delta$, which leads to $f(\omega) < 1$. Thus, it is mainly the counterrotating term in $f(\omega)$ that reduces the effect of the energy peak of the bath on the decay. This slows down the decay and only the quantum Zeno effect can now take place. The projection-intervals-modulating function $F(\omega,\tau)$, together with the interaction-modulating function $f(\omega)$, causes the Zeno effect to dominate in the high-frequency-cutoff Ohmic bath. A summary of results of this section is shown in Table I.

IV. SUMMARY

In summary, we have studied a model of a qubit interacting with its environment, modeled either as a low- or as a high-frequency bath. For each type of bath, the quantum dynamics of the qubit without measurement and the quantum Zeno effect on it are shown for the cases of weak and strong couplings between the qubit and the environment. Our results show that, for a low-frequency bath, the qubit energy increases (blue shift) and the quantum anti-Zeno effect occurs. However, for a high-frequency-cutoff Ohmic bath, the qubit energy decreases (red shift) and the quantum Zeno effect dominates. Moreover, under the condition of equal decay rate due to the two kinds of baths in the WW approximation, for a high-frequency environment, we find that without the approximation, the decay rate should be faster (without measurements) or slower (with frequent measurements, in the Zeno regime), compared to the low-frequency-bath case. These very different behaviors of the quantum dynamics and the Zeno effect in different baths should be helpful to experimentally distinguish the type of noise affecting the qubit and protect the coherence of the qubit through modulating the dominant frequency of its environment.

ACKNOWLEDGMENTS

We are very grateful to Adam Miranowicz for his very helpful comments. FN acknowledges partial support from the Laboratory of Physical Sciences, National Security Agency, Army Research Office, National Science Foundation Grant No. 0726909, JSPS-RFBR Contract No. 09-02-92114, Grant-in-Aid for Scientific Research (S), MEXT Kakenhi on Quantum Cybernetics, and the Funding Program for Innovative R&D on S&T (FIRST). XC acknowledges support from the National Natural Science Foundation of China under Grant No. 10904126 and Fujian Province Natural Science Foundation under Grant No. 2009J05014. JQY acknowledges partial support from the National Natural Science Foundation of China under Grant No. 10625416, the National Basic Research Program of China under Grant No. 2009CB929300, and the ISTCP under Grant No. 2008DFA01930.

APPENDIX: EXAMINING THE VALIDITY OF THE UNITARY TRANSFORMATION

In this Appendix, we show the main results of the canonical transformation to the qubit-bath Hamiltonian H considered here, and we prove that the contribution of H_2' to physical quantities is of $O(g_k^4)$ and higher, so we ignore H_2' in the calculations. We now apply a canonical transformation to the Hamiltonian H as in Eq. (3):

$$H' = \exp(S) H \exp(-S), \tag{A1}$$

with

$$S = \sum_k \frac{\chi_k}{2}(a_k^\dagger - a_k)\sigma_x. \tag{A2}$$

Here we define $\chi_k = g_k\xi_k/\omega_k$, which is proportional to g_k. A k-dependent variable χ_k is introduced in the transformation. It is clear that this canonical transformation is unitary, because $[\exp(S)]^\dagger = \exp(-S)$. The transformed Hamiltonian H' can now be decomposed in three parts:

$$H' = H'_0 + H'_1 + H'_2, \tag{A3}$$

with

$$H'_0 = -\frac{1}{2}\eta\ \Delta\sigma_z + \sum_k \omega_k a_k^\dagger a_k - \sum_k \frac{g_k}{4}\chi_k(2-\xi_k), \tag{A4}$$

$$H'_1 = \sum_k \eta\ \Delta\chi_k(a_k^\dagger\sigma_- + a_k\sigma_+), \tag{A5}$$

$$H'_2 = -\frac{1}{2}\Delta\sigma_z(\cos Y - \eta) + \frac{\Delta}{2}\sigma_y(-\sin Y + \eta Y), \tag{A6}$$

where, in Eq. (A6),

$$Y = i\sum_k \chi_k(a_k^\dagger - a_k) \tag{A7}$$

is a generalized momentum and η is defined in Eq. (4), $\eta = \exp(-\sum_k \chi_k^2/2)$.

Note that no approximation was used during the transformation, so $H' = \exp[S]H\exp[-S]$ is exact. Because the constant term $\sum_k g_k\chi_k(2-\xi_k)/4$ in Eq. (A4) has no effect on the dynamical evolution, we neglect it. At low temperatures, the multiple-step process is so weak that all the higher-order terms can be neglected. In the following derivation, we will prove that the contribution of H'_2 to physical quantities is of $O(g_k^4)$ and higher, so we ignore H'_2 and obtain the effective transformed Hamiltonian $H' = H'_0 + H'_1$.

Now let us expand the first term of H'_2, $\cos Y$, as a series in χ_k. Using the Baker-Hausdorff theorem, we have

$$\exp\left(\sum_k \chi_k(a_k^\dagger - a_k)\right) \tag{A8}$$

$$= \eta\exp\left(\sum_k \chi_k a_k^\dagger\right)\exp\left(\sum_k -\chi_k a_k\right). \tag{A9}$$

Afterward, we expand (A9) as follows:

$$\eta\exp\left(\sum_k \chi_k a_k^\dagger\right)\exp\left(\sum_k -\chi_k a_k\right)$$
$$= \eta\left[1 + \sum_k \chi_k a_k^\dagger + \frac{\left(\sum_k \chi_k a_k^\dagger\right)^2}{2} + \frac{\left(\sum_k \chi_k a_k^\dagger\right)^3}{3!} + \cdots\right]$$
$$\times\left[1 - \sum_k \chi_k a_k + \frac{\left(\sum_k \chi_k a_k\right)^2}{2} - \frac{\left(\sum_k \chi_k a_k\right)^3}{3!} + \cdots\right]$$
$$= \eta\left[1 + \sum_k \chi_k a_k^\dagger - \sum_k \chi_k a_k - \sum_k \chi_k a_k^\dagger \sum_k \chi_k a_k + \cdots\right]. \tag{A10}$$

Now we see the second-order terms in χ_k in this equation:

$$\left(\sum_k \chi_k a_k^\dagger\right)\left(\sum_k \chi_k a_k\right)$$
$$= \sum_k \chi_k^2 a_k^\dagger a_k(\text{diagonal}) + \sum_{k\neq k'} \chi_k a_k^\dagger \chi_{k'} a_{k'}(\text{off-diagonal}). \tag{A11}$$

The off-diagonal terms are related to the multiboson transition and their contributions to the physical quantities are fourth order in χ_k. Furthermore, the initial state $|\{0_k\}\rangle|\uparrow\rangle$ is used in the calculation, so the direct effect of the second-order diagonal term on physical quantities is zero and its effect through the interaction will also be fourth order in χ_k. Thus we now ignore the terms higher than second order in χ_k in the following calculation and obtain the expression of (A8):

$$\exp\left[\sum_k \chi_k(a_k^\dagger - a_k)\right] \approx \eta\left(1 + \sum_k \chi_k a_k^\dagger - \sum_k \chi_k a_k\right). \tag{A12}$$

Therefore, $\cos Y$ is reduced to

$$\cos Y \approx \eta. \tag{A13}$$

In the same way, $\sin Y$ in H'_2 is simplified to

$$\sin Y \approx \eta\left[Y + O\left(\chi_k^3\right)\right]. \tag{A14}$$

In H'_2, we have subtracted the terms of zero and first order in g_k, which are included in $H'_0 + H'_1$, and only left the terms equal to and higher than second order in g_k, whose contribution to the physical quantities is of $O(g_k^4)$ and higher. Thus, H'_2 can be omitted.

We expand several series in the variable χ_k, while the real variable is $\eta\Delta\chi_k$. Because $\eta\Delta\chi_k = \eta\Delta g_k\xi_k/\omega_k = \eta\Delta g_k/(\omega_k + \eta\Delta) < g_k$, then $\eta\Delta\chi_k$ is less than g_k. In other words, through this transformation we find a variable smaller than g_k for the series expansion. Therefore, our method can be extended to the case of strong interaction between the qubit and the environment.

[1] R. McDermott, IEEE Trans. Appl. Supercond. **19**, 2 (2009).
[2] J. Q. You and F. Nori, Phys. Today **58**, 42 (2005).
[3] J. Clarke and F. K. Wilhelm, Nature (London) **453**, 1031 (2008).
[4] F. Yoshihara, K. Harrabi, A. O. Niskanen, Y. Nakamura, and J. S. Tsai, Phys. Rev. Lett. **97**, 167001 (2006).
[5] K. Kakuyanagi, T. Meno, S. Saito, H. Nakano, K. Semba, H. Takayanagi, F. Deppe, and A. Shnirman, Phys. Rev. Lett. **98**, 047004 (2007).
[6] A. N. Omelyanchouk, S. Savel'ev, A. M. Zagoskin, E. Il'ichev, and F. Nori, Phys. Rev. B **80**, 212503 (2009).
[7] R. H. Koch, D. P. DiVincenzo, and J. Clarke, Phys. Rev. Lett. **98**, 267003 (2007).
[8] R. de Sousa, Phys. Rev. B **76**, 245306 (2007).
[9] L. Faoro and L. B. Ioffe, Phys. Rev. Lett. **100**, 227005 (2008).
[10] L. Zhou, S. Yang, Y. X. Liu, C. P. Sun, and F. Nori, Phys. Rev. A **80**, 062109 (2009).
[11] C. Search and P. R. Berman, Phys. Rev. Lett. **85**, 2272 (2000).

[12] S. Maniscalco, F. Francica, R. L. Zaffino, N. Lo Gullo, and F. Plastina, Phys. Rev. Lett. **100**, 090503 (2008).
[13] X.-B. Wang, J. Q. You, and F. Nori, Phys. Rev. A **77**, 062339 (2008).
[14] N. Erez, G. Gordon, M. Nest, and G. Kurizki, Nature (London) **452**, 724 (2008).
[15] A. G. Kofman and G. Kurizki, Nature (London) **405**, 546 (2000).
[16] P. Facchi and S. Pascazio, Phys. Rev. A **62**, 023804 (2000); Phys. Lett. A **241**, 139 (1998); P. Facchi, H. Nakazato, and S. Pascazio, Phys. Rev. Lett. **86**, 2699 (2001).
[17] E. Block and P. R. Berman, Phys. Rev. A **44**, 1466 (1991).
[18] G. S. Agarwal, *Quantum Statistical Theories of Spontaneous Emission and Their Relation to Other Approaches* (Springer-Verlag, Berlin, 1974).
[19] A. G. Kofman and G. Kurizki, Phys. Rev. Lett. **93**, 130406 (2004).
[20] D. P. Di Vincenzo and D. Loss, Phys. Rev. B **71**, 035318 (2005).
[21] G. Burkard, Phys. Rev. B **79**, 125317 (2009).
[22] X.-F. Cao and H. Zheng, Phys. Rev. A **77**, 022320 (2008); P.-H. Huang and H. Zheng, J. Phys.: Condens. Matter **20**, 395233 (2008); X.-F. Cao and H. Zheng, Phys. Rev. B **76**, 115301 (2007); Z.-G. Lü and H. Zheng, *ibid.* **75**, 054302 (2007).
[23] G. Gordon, G. Bensky, D. Gelbwaser-Klimovsky, D. D. B. Rao, N. Erez, and G. Kurizki, New J. Phys. **11**, 123025 (2009).
[24] U. Weiss, *Quantum Dissipative Systems*, 3rd ed. (World Scientific, Singapore, 2008).
[25] X.-F. Cao and H. Zheng, Phys. Rev. A **75**, 062121 (2007).
[26] S. De Liberato, D. Gerace, I. Carusotto, and C. Ciuti, Phys. Rev. A **80**, 053810 (2009).
[27] H. Zheng, Eur. Phys. J. B **38**, 559 (2004).
[28] S. Ashhab, J. Q. You, and F. Nori, Phys. Rev. A **79**, 032317 (2009); New J. Phys. **11**, 083017 (2009); Phys. Scr. T **137**, 014005 (2009).
[29] Q. Ai, D.-Z. Xu, S. Yi, A. G. Kofman, C. P. Sun, and F. Nori, e-print arXiv:1007.4859 (2010).
[30] H. Zheng, S. Y. Zhu, and M. S. Zubairy, Phys. Rev. Lett. **101**, 200404 (2008).
[31] Z.-H. Li, D.-W. Wang, H. Zheng, S.-Y. Zhu, and M. S. Zubairy, Phys. Rev. A **80**, 023801 (2009).
[32] G. Ithier, E. Collin, P. Joyez, P. J. Meeson, D. Vion, D. Esteve, F. Chiarello, A. Shnirman, Y. Makhlin, J. Schriefl, and G. Schön, Phys. Rev. B **72**, 134519 (2005).